

Dependence of UO₂ Surface Morphology on Processing History within a Single Synthetic Route

Erik C. Abbott^a, Alexandria Brenkmann^a, Craig Galbraith^a, Joshua Ong^b, Ian J. Schwerdt^a, Brent D. Albrecht^b, Tolga Tasdizen^b Luther W. McDonald IV^a

^aUniversity of Utah Department of Civil and Environmental Engineering-Nuclear Engineering Program, 201 Presidents Circle, Salt Lake City, UT 84112, United States

^bUniversity of Utah Scientific Computing and Imaging Institute, 72 S Central Campus Drive, Salt Lake City, UT 84112, United States

Corresponding Author: Luther W. McDonald. 110 Central Campus Dr. Suite 2000, Salt Lake City, UT 84112. Luther.mcdonald@utah.edu, 801-581-7768

KEYWORDS. Nuclear Forensics, Morphology, X-ray Diffraction, X-ray Photoelectron Spectroscopy, Scanning Electron Microscopy

Table of Contents

Table S-1. X-ray Photoelectron Spectroscopy Scan Settings	3
Table S-2. Machine Learning Training Modules.....	4
Figure S-1. Intermediate U-oxides and Resulting UO_2	5
Figure S-2. SEM Image of UO_2 Synthesized from Am- UO_3	6
Figure S-3. SEM Image of UO_2 Synthesized from Am- UO_3	7
Figure S-4. SEM Image of UO_2 Synthesized from Am- UO_3	8
Figure S-5. SEM Image of UO_2 Synthesized from Am- UO_3	9
Figure S-6. SEM Image of UO_2 Synthesized from Am- UO_3	10
Figure S-7. SEM Image of UO_2 Synthesized from Am- UO_3	11
Figure S-8. SEM Image of UO_2 Synthesized from α - UO_3	12
Figure S-9. SEM Image of UO_2 Synthesized from α - UO_3	13
Figure S-10. SEM Image of UO_2 Synthesized from α - UO_3	14
Figure S-11. SEM Image of UO_2 Synthesized from α - UO_3	15
Figure S-12. SEM Image of UO_2 Synthesized from α - UO_3	16
Figure S-13. SEM Image of UO_2 Synthesized from α - UO_3	17
Figure S-14. SEM Image of UO_2 Synthesized from U_3O_8	18
Figure S-15. SEM Image of UO_2 Synthesized from U_3O_8	19
Figure S-16. SEM Image of UO_2 Synthesized from U_3O_8	20
Figure S-17. SEM Image of UO_2 Synthesized from U_3O_8	21
Figure S-18. SEM Image of UO_2 Synthesized from U_3O_8	22
Figure S-19. SEM Image of UO_2 Synthesized from U_3O_8	23
Figure S-20. Segmented Image of Am- UO_3	24
Figure S-21. Segmented Image of U_3O_8	25
Figure S-22. Segmented image of UO_2 synthesized from Am- UO_3	26
Figure S-23. Segmented image of UO_2 synthesized from U_3O_8	27

Table S-1. X-ray Photoelectron Spectroscopy scan settings which were used during each scan. The Charge Neutralize Test was used to determine the need to use the electron gun to manage the effects of charging. The low-resolution Survey scan was used to identify which elements were present in the sample. The high-resolution scan for each element were for analysis.

Scan	Pass Energy (eV)	Scan Range (eV)	Step Size (eV)	Dwell Time (ms)	Sweeps
Charge Neutralize Test	40	270-300	0.1	150	1
Survey	160	0-1400	1	100	1
O 1s	40	520-545	0.1	500	1
U 4f	40	360-420	0.1	500	1
C 1s	40	270-295	0.1	500	1

Table S-2. Machine Learning training modules which were used to train and evaluate the data. These data were partitioned into different bins and trained and evaluated using five different models and shown in the table.

	Bin 1	Bin 2	Bin 3	Bin 4	Bin 5
Fold 1	Train	Train	Train	Train	Evaluate
Fold 2	Train	Train	Train	Evaluate	Train
Fold 3	Train	Train	Evaluate	Train	Train
Fold 4	Train	Evaluate	Train	Train	Train
Fold 5	Evaluate	Train	Train	Train	Train

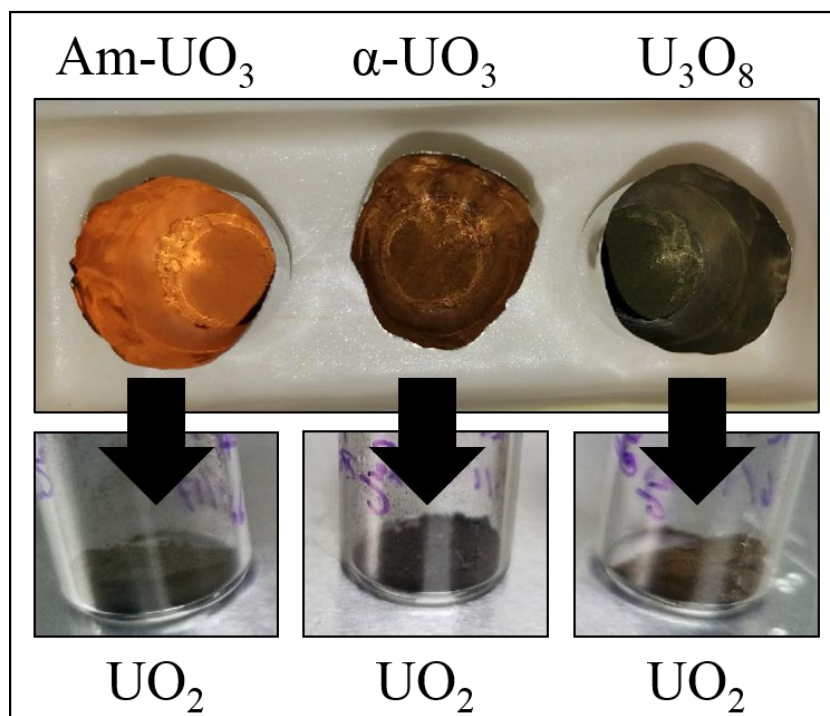


Figure S-1. Intermediate U-oxides and resulting UO_2 . Am- UO_3 (top left), α - UO_3 (top center), and U_3O_8 (top right) were simultaneously reduced to UO_2 via hydrogen reduction in the same atmosphere controlled furnace. A 50:50 mixture of H_2 and He were flowed through the furnace at 500 mL/min for 5 hours at 510 °C. The resulting UO_2 (bottom) are shown above.

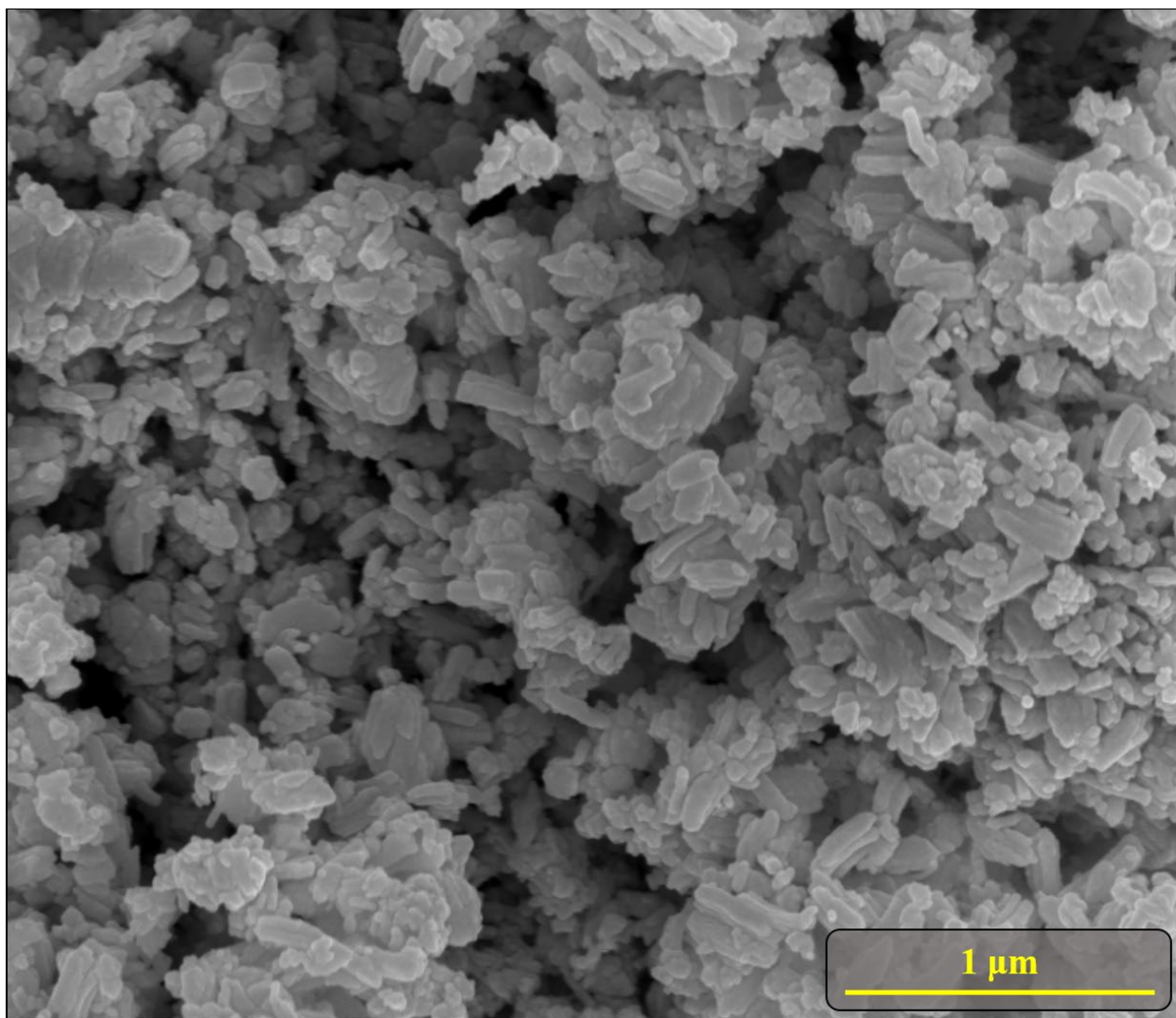


Figure S-2. SEM image representative of the UO₂ synthesized from Am-UO₃. The nanoparticles of these samples consist of a bimodal distribution. One mode is comprised of large elongated particles with well-rounded edges and low sphericity, while the other mode is comprised of much smaller, rounded particles with well-rounded edges moderate sphericity. Particles from each mode vary widely in size and shape. The morphology of the UO₂ synthesized from Am-UO₃ closely resembles the morphology of the Am-UO₃ from which it was made.

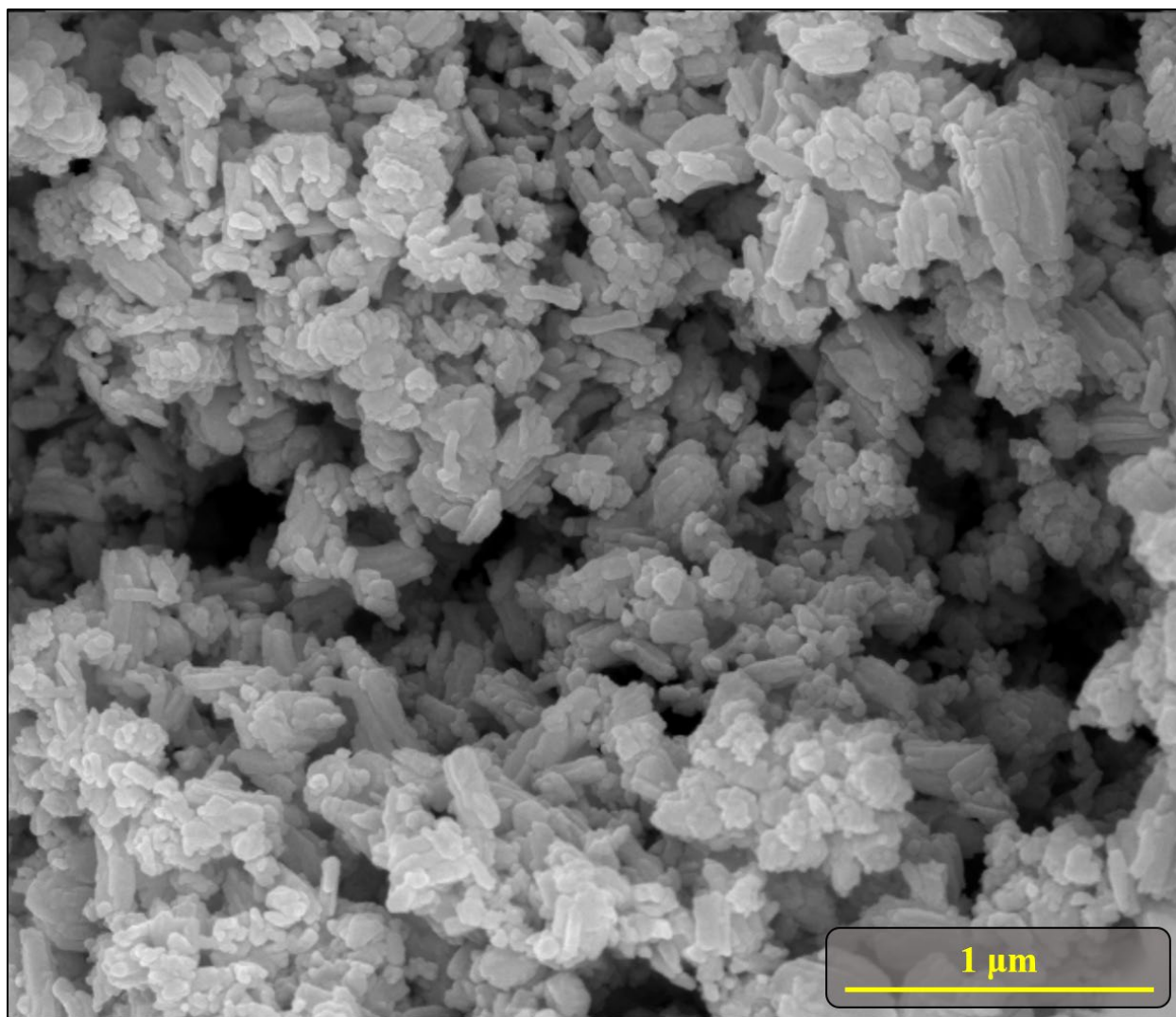


Figure S-3. SEM image representative of the UO₂ synthesized from Am-UO₃ exhibiting the morphology and bimodal distribution discussed in Figure S-2.

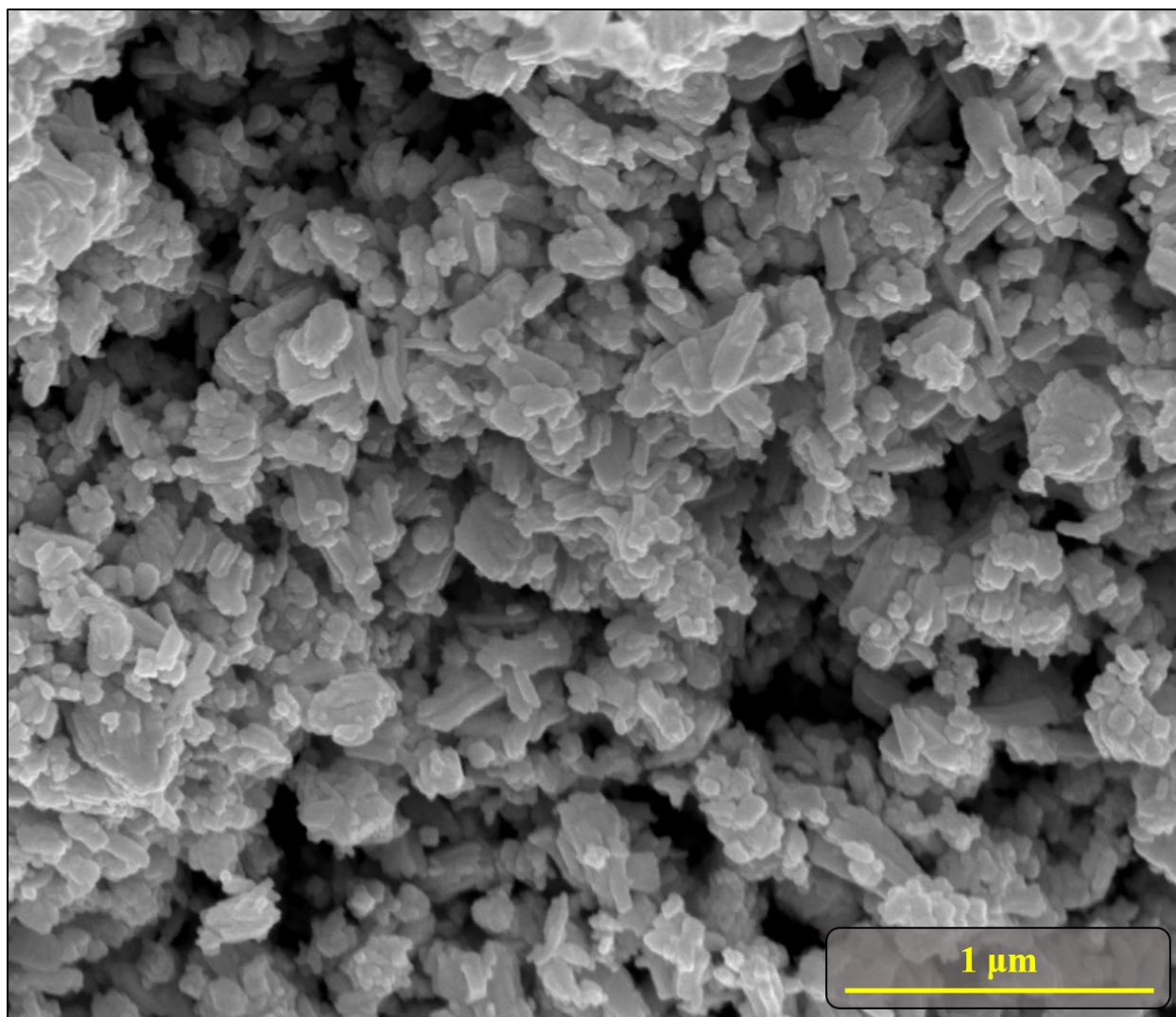


Figure S-4. SEM image representative of the morphology of UO_2 synthesized from Am-UO_3 as described in Figure S-2.

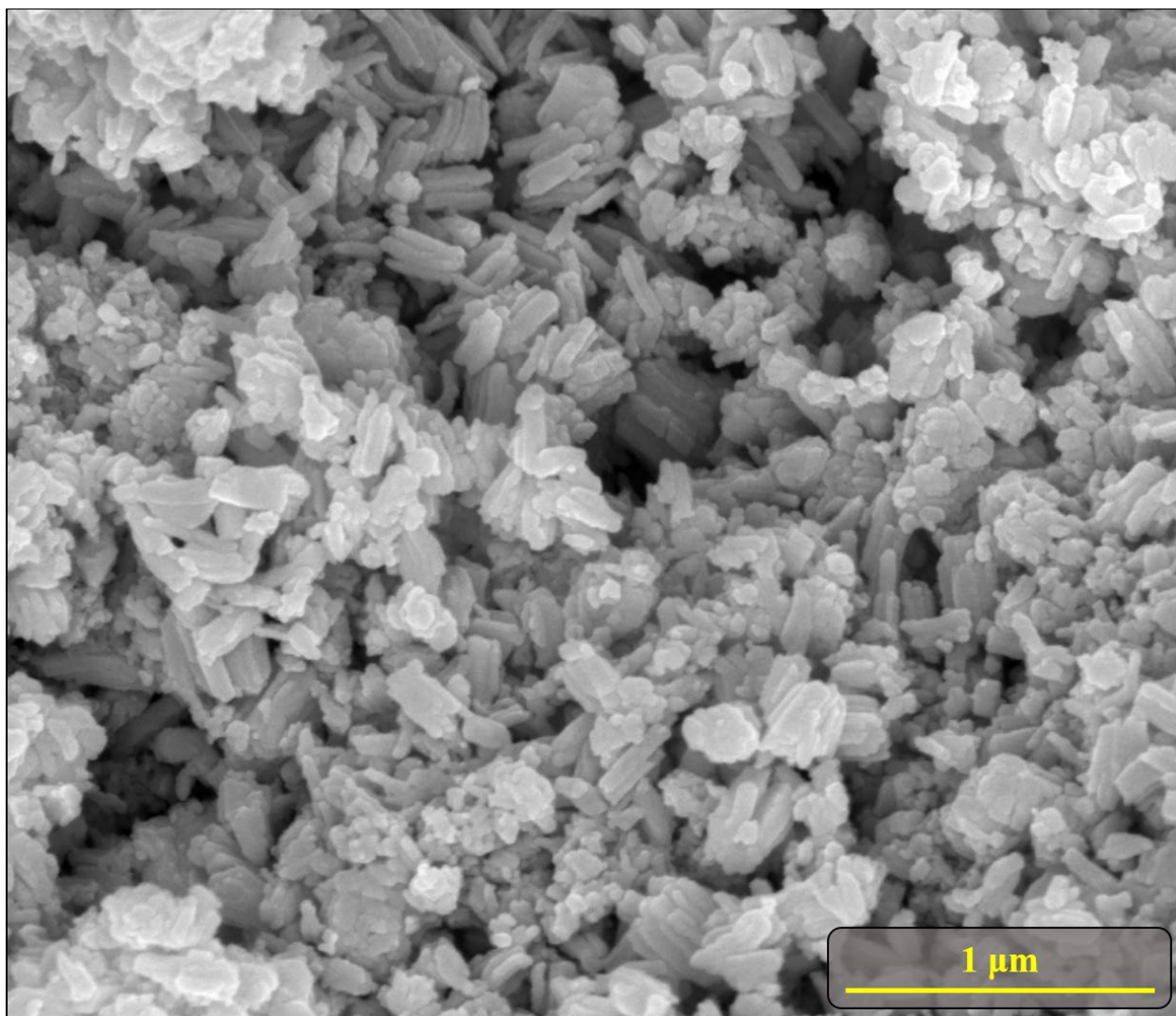


Figure S-5. SEM image representative of the UO₂ synthesized from Am-UO₃ as described in Figure S-2 with good examples of the larger elongated particles and small rounded particles.

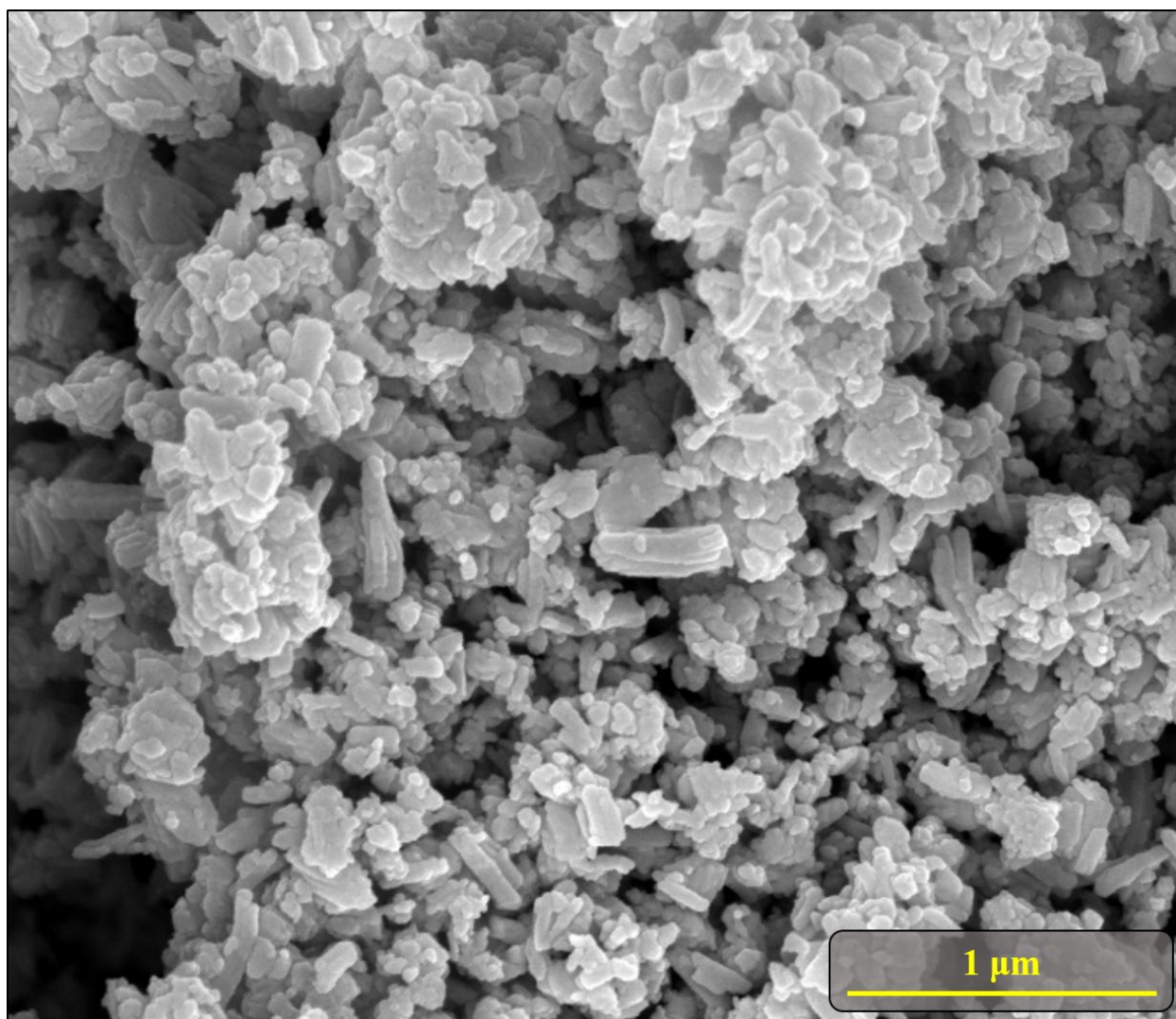


Figure S-6. SEM image representative of the morphology of UO₂ synthesized from Am-UO₃ described in Figure S-2 which highlights the bimodal nature of the morphology.

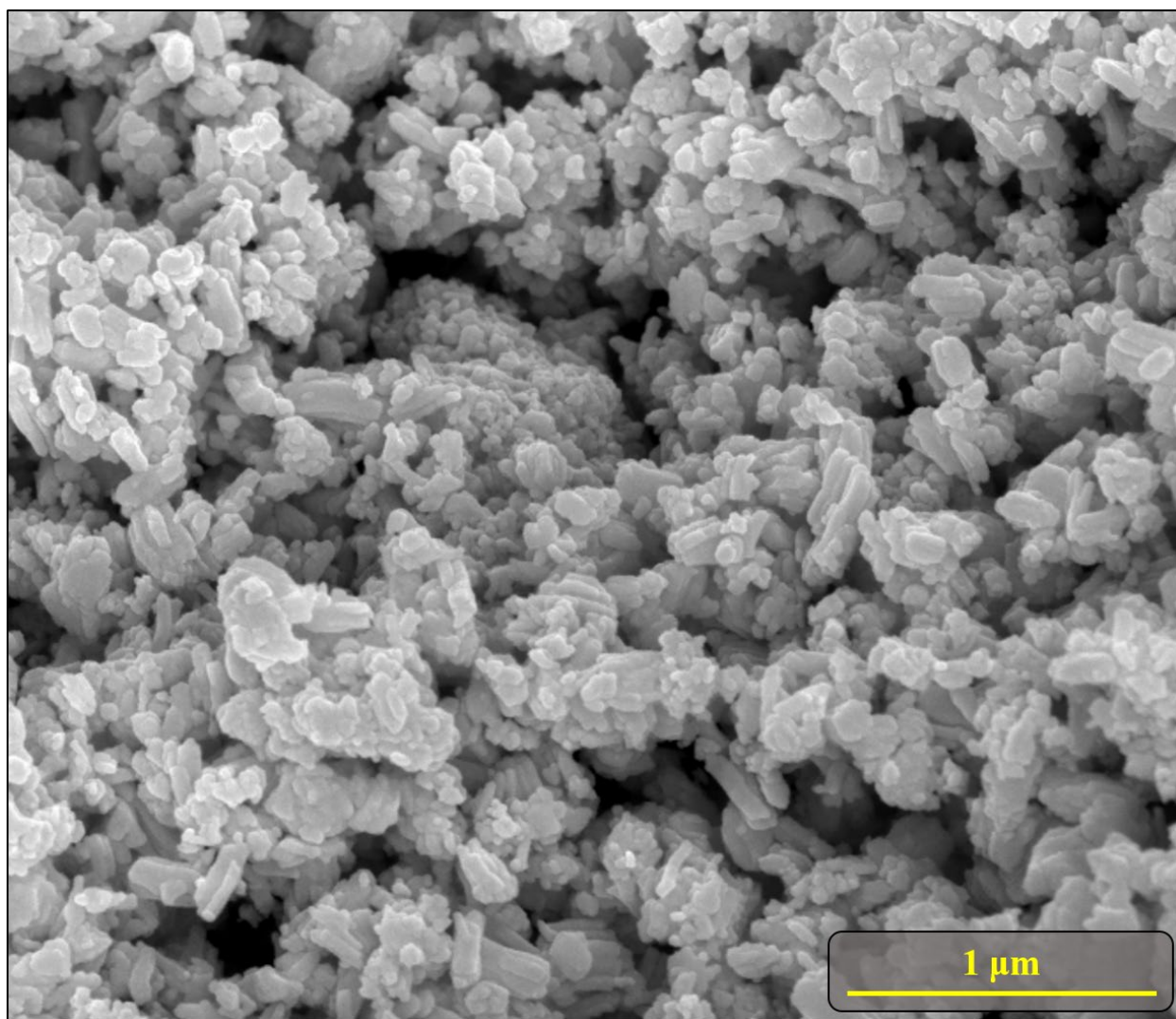


Figure S-7. SEM image representative of the morphology of UO₂ synthesized from Am-UO₃ as described in Figure S-2 and highlights the smaller rounded particles, though there is still an abundance of the larger elongated particles.

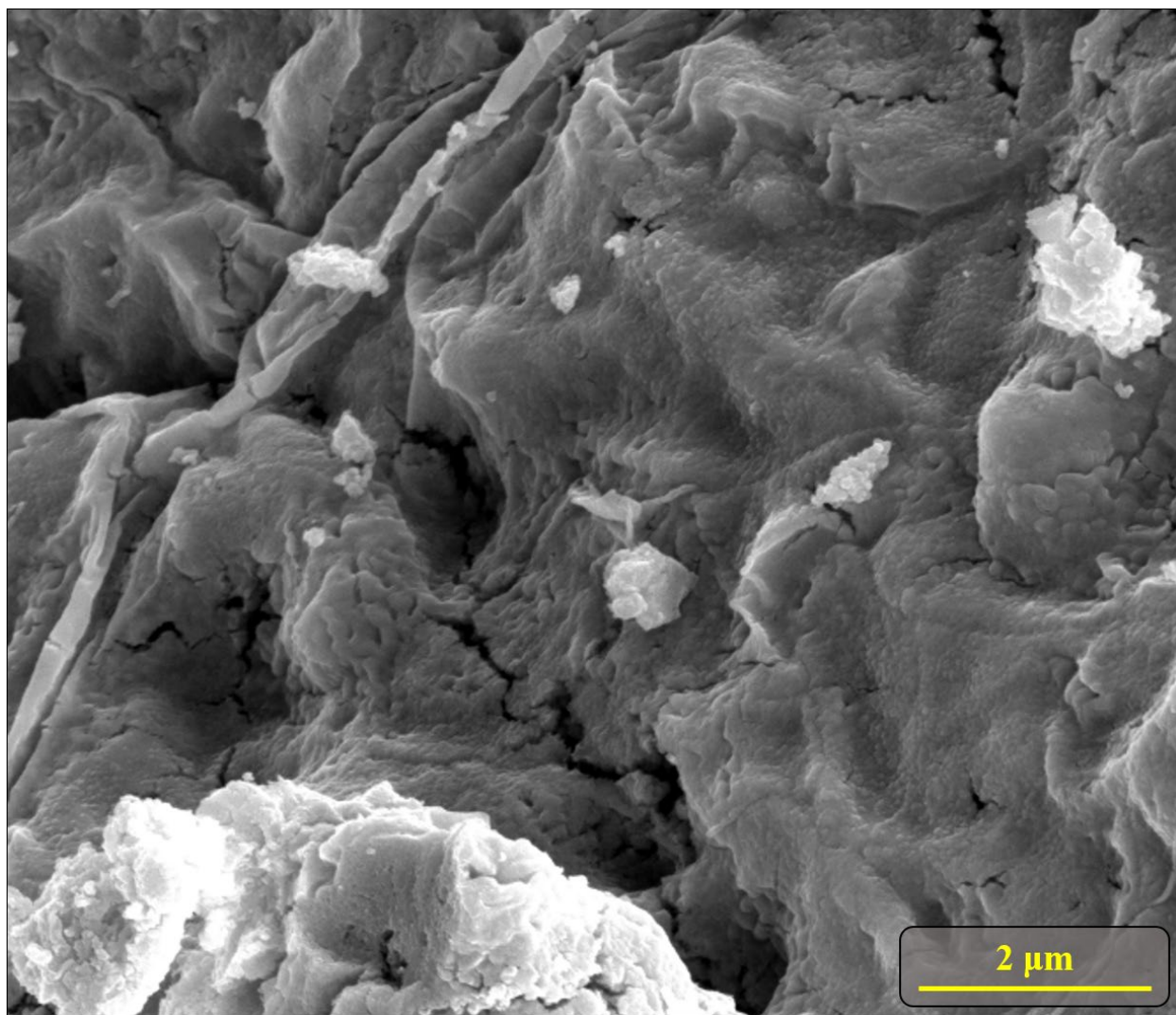


Figure S-8. SEM image representative of UO₂ synthesized from α -UO₃. The morphology of these particles is complicated, and the morphology is inconsistent even on the same particle. The morphology of the UO₂ synthesized from α -UO₃ resembles the α -UO₃ from which it was made. In this image a variety of morphologies are observed including concave surfaces which smooth in some areas, rough in some area, or ornamented in others with rounded discs. This images also shows several rough surface fractures, irregular blocky surface particles with angular edges, and even smooth ribbons with rounded edges.

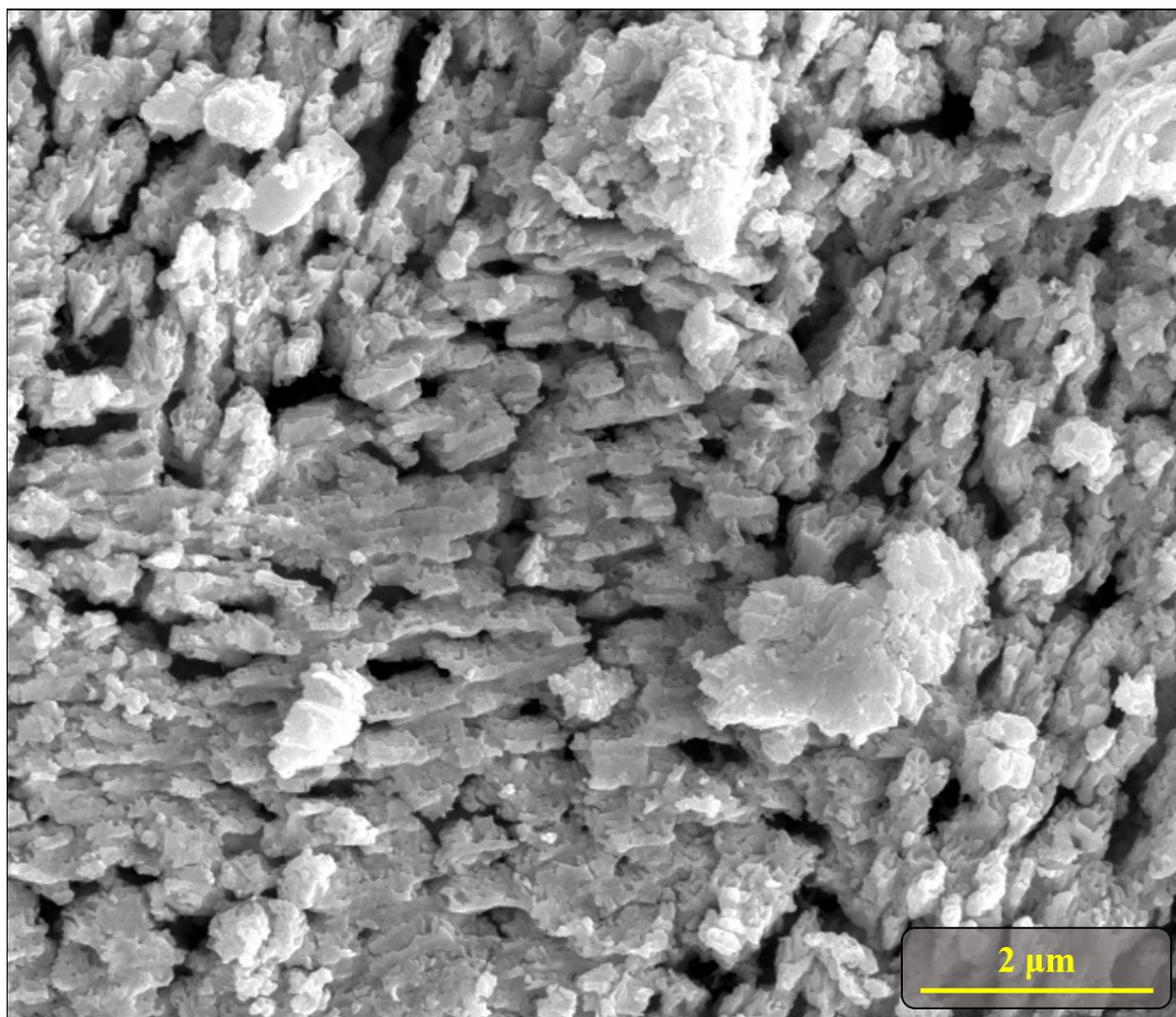


Figure S-9. SEM image representative of the morphology of UO_2 synthesized from $\alpha\text{-UO}_3$. This image highlights the presence of both polyhedral and irregular surface particles with very angular edges.

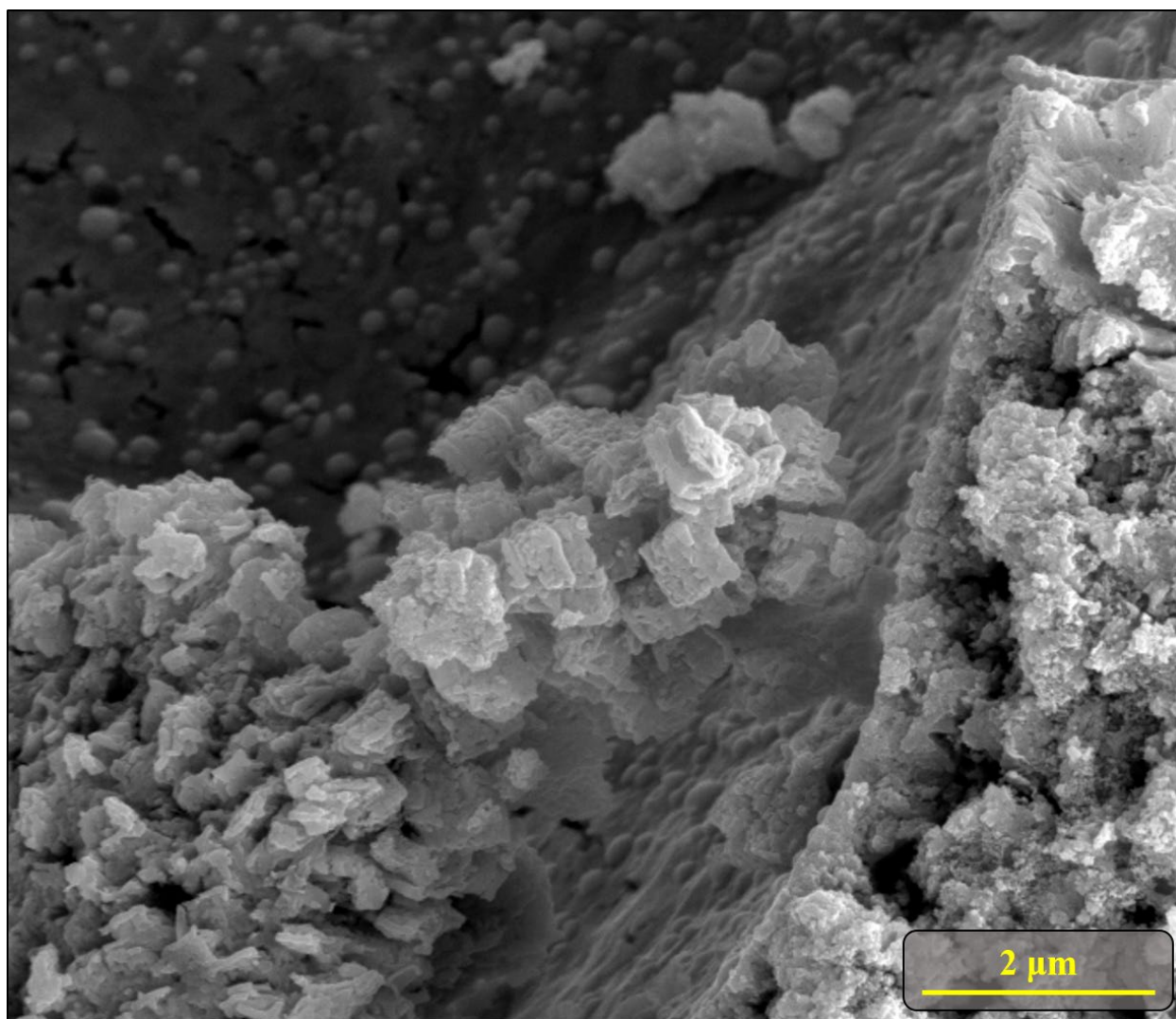


Figure S-10. SEM image representative of the morphology of UO_2 synthesized from $\alpha\text{-UO}_3$. This image shows the presence of flat surface with rounded, spherical surface ornaments, surface fractures, polyhedral, columnar surface particles with angular edges, and small rounded particles with moderate sphericity.

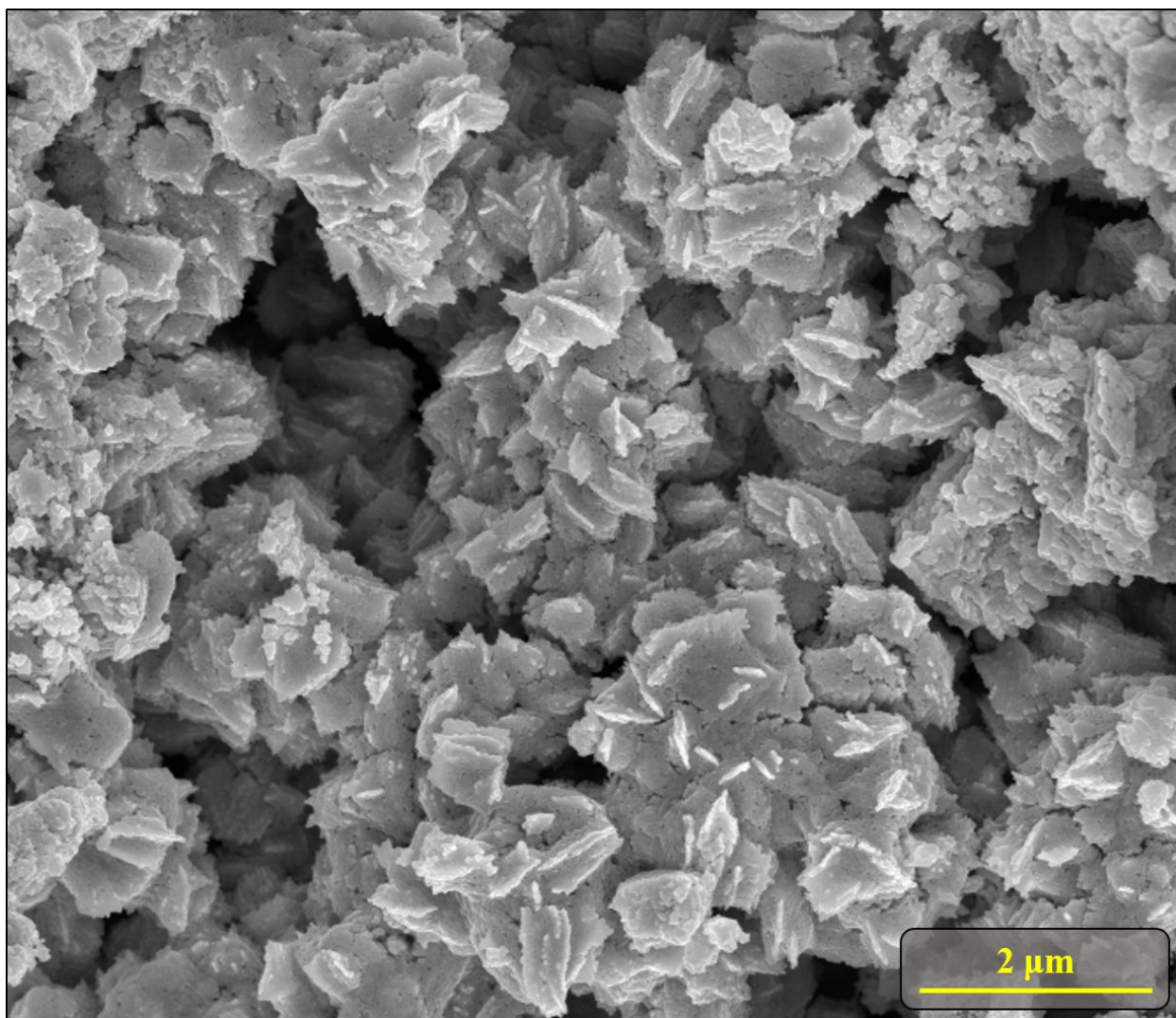


Figure S-11. SEM image representative of UO_2 synthesized from $\alpha\text{-UO}_3$. The morphology in this image features flat blades and irregular, blocky surface particles with very angular edges.

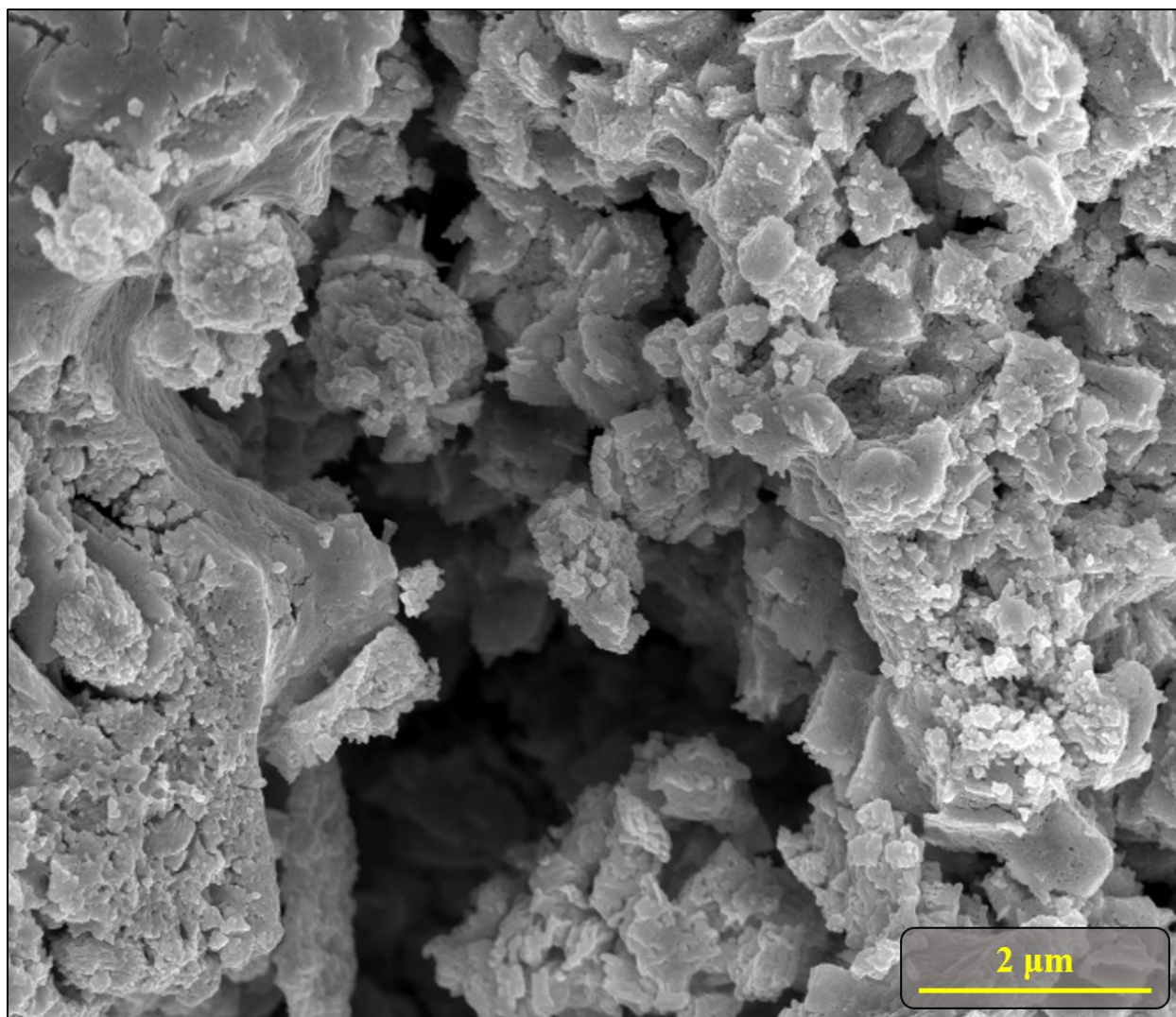


Figure S-12. SEM image representative of UO_2 synthesized from $\alpha\text{-UO}_3$. The morphology of this image is representative of smooth concave surfaces, large, irregular, blocky surface particles, flat blades, and small rounded particles.

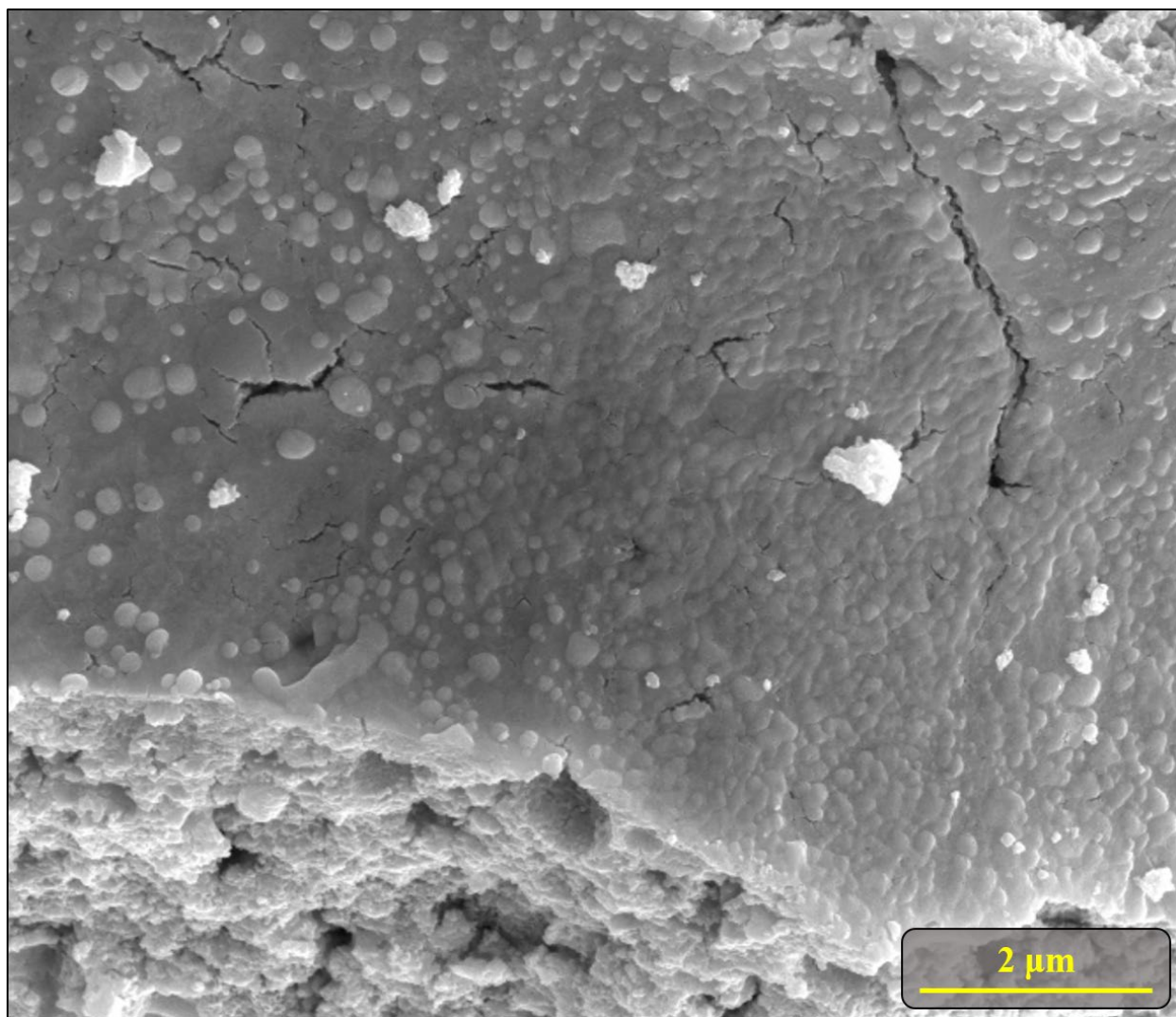


Figure S-13. SEM image representative of the morphology of UO₂ synthesized from α-UO₃. the bulk of this image is a smooth flat surface with surface ornamentation characterized by rounded discs, and also featuring surface cracks and irregular surface particles. The smooth surface appears to be a crust, and the morphology of the underlying particle is very rough.

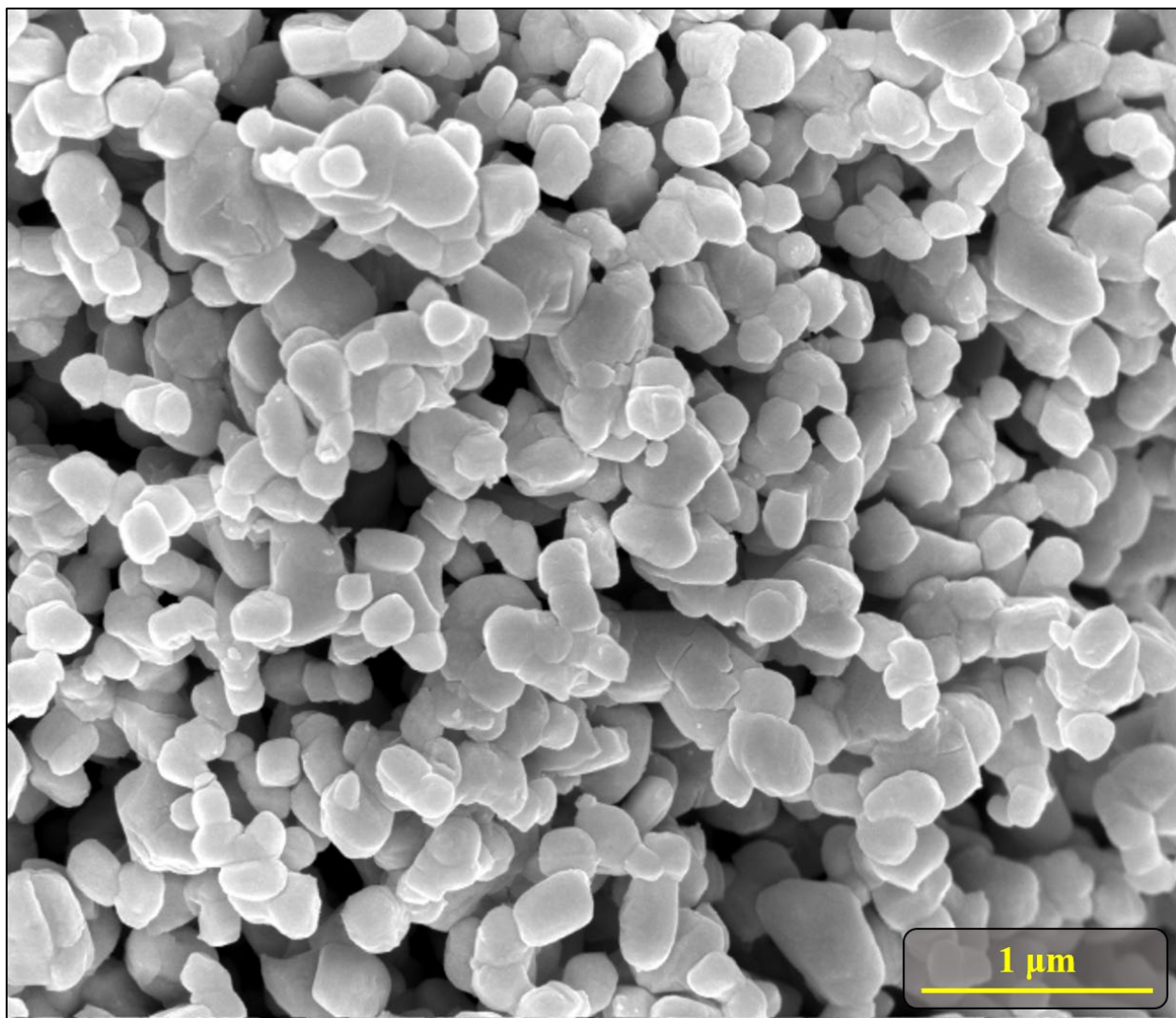


Figure S-14. SEM image representative of UO₂ synthesized from U₃O₈. The morphology of these particles have a morphology which consists of smooth, rounded particles with well-rounded edges and moderate sphericity. They are larger, have higher circularity, and greater uniformity in size and shape than the UO₂ synthesized from Am-UO₃. The morphology of the UO₂ synthesized from U₃O₈ resembles the morphology of the U₃O₈ from which it was made.

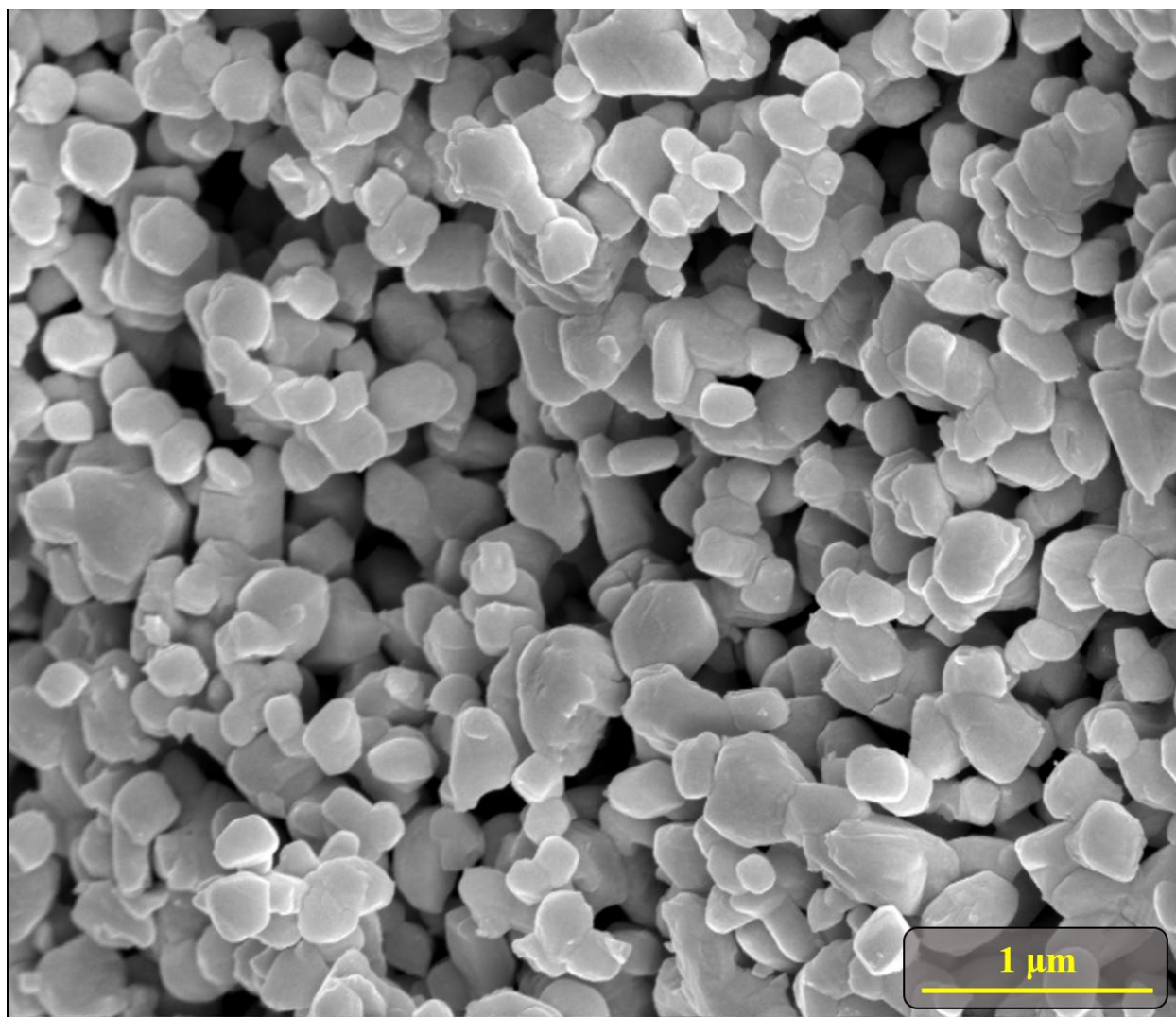


Figure S-15. SEM image representative of the morphology of UO_2 synthesized from U_3O_8 as described in Figure S-14.

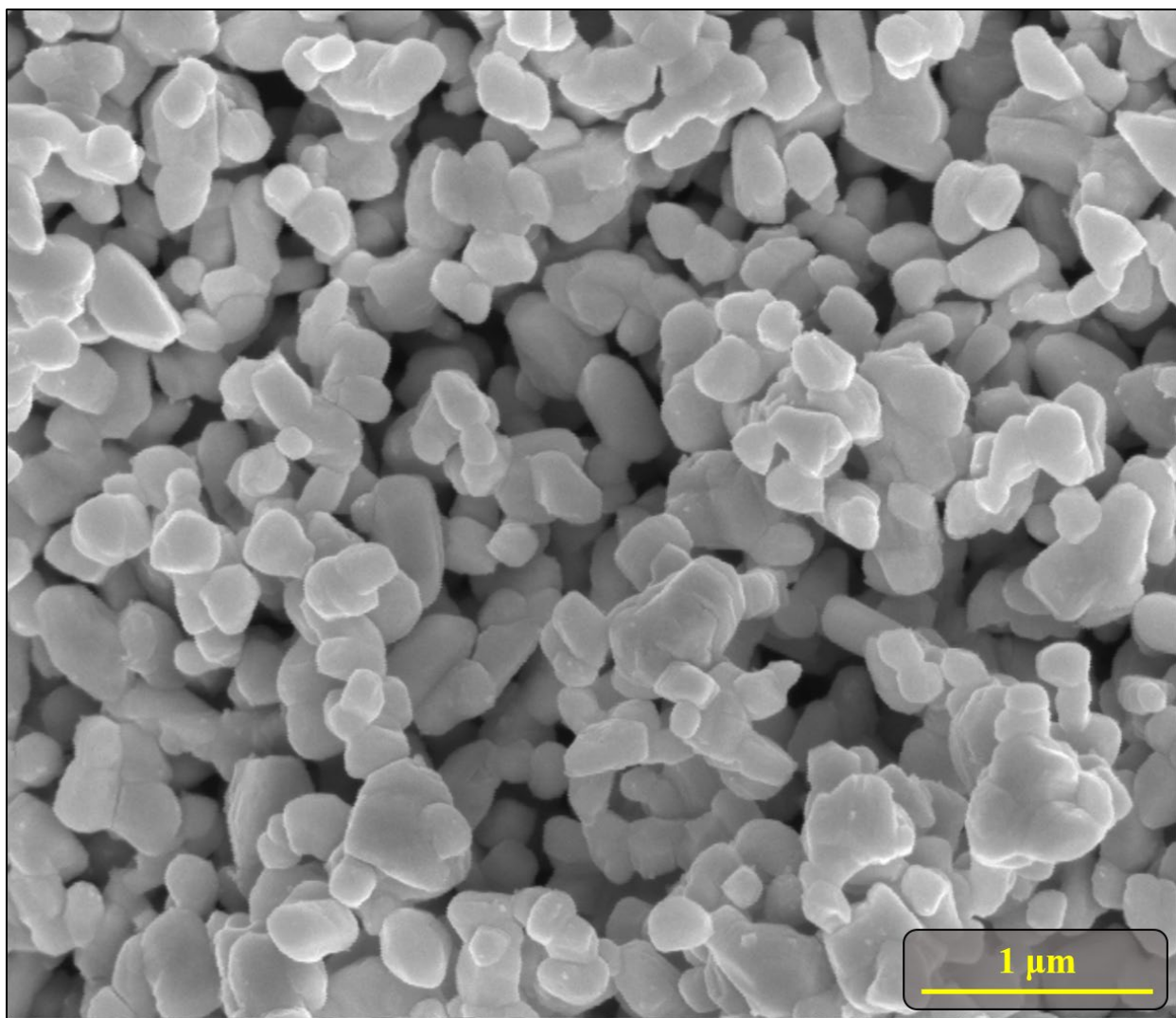


Figure S-16. SEM image representative of UO₂ synthesized from U₃O₈ with morphology described in Figure S-14.

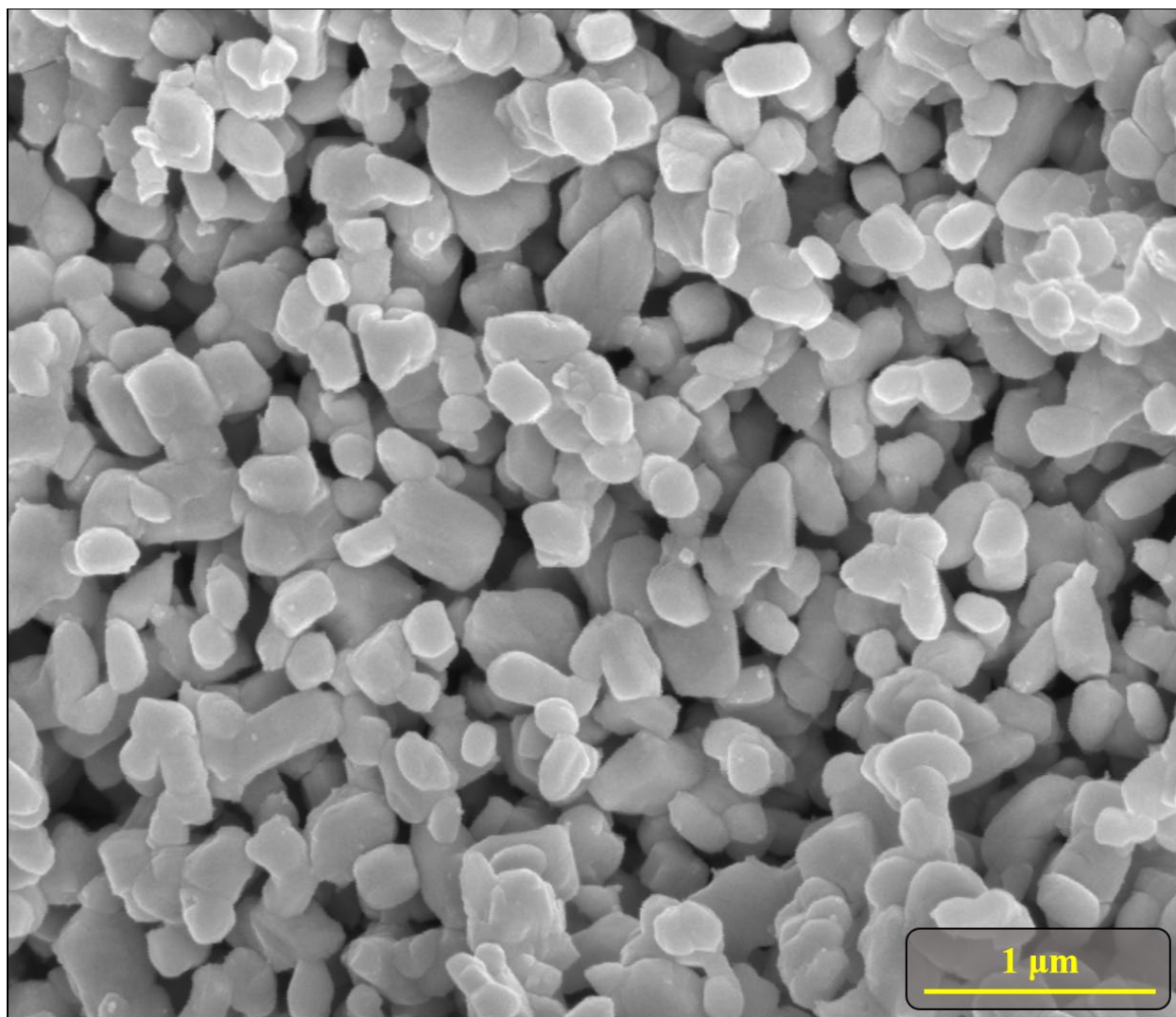


Figure S-17. SEM image representative of the morphology of UO₂ synthesized from U₃O₈ as described in Figure S-14.

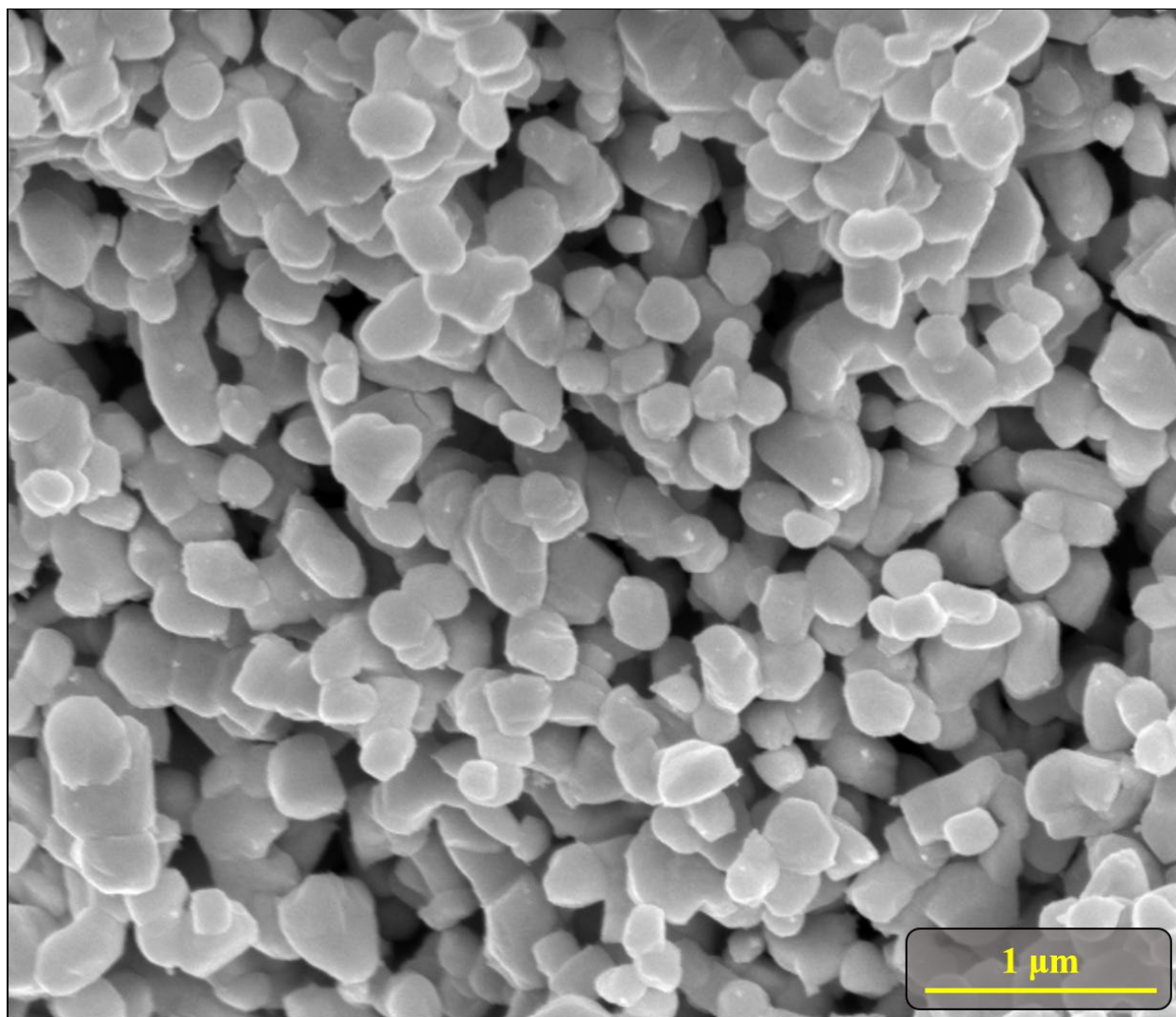


Figure S-18. SEM image representative of the morphology of UO_2 synthesized from U_3O_8 as described in Figure S-14.

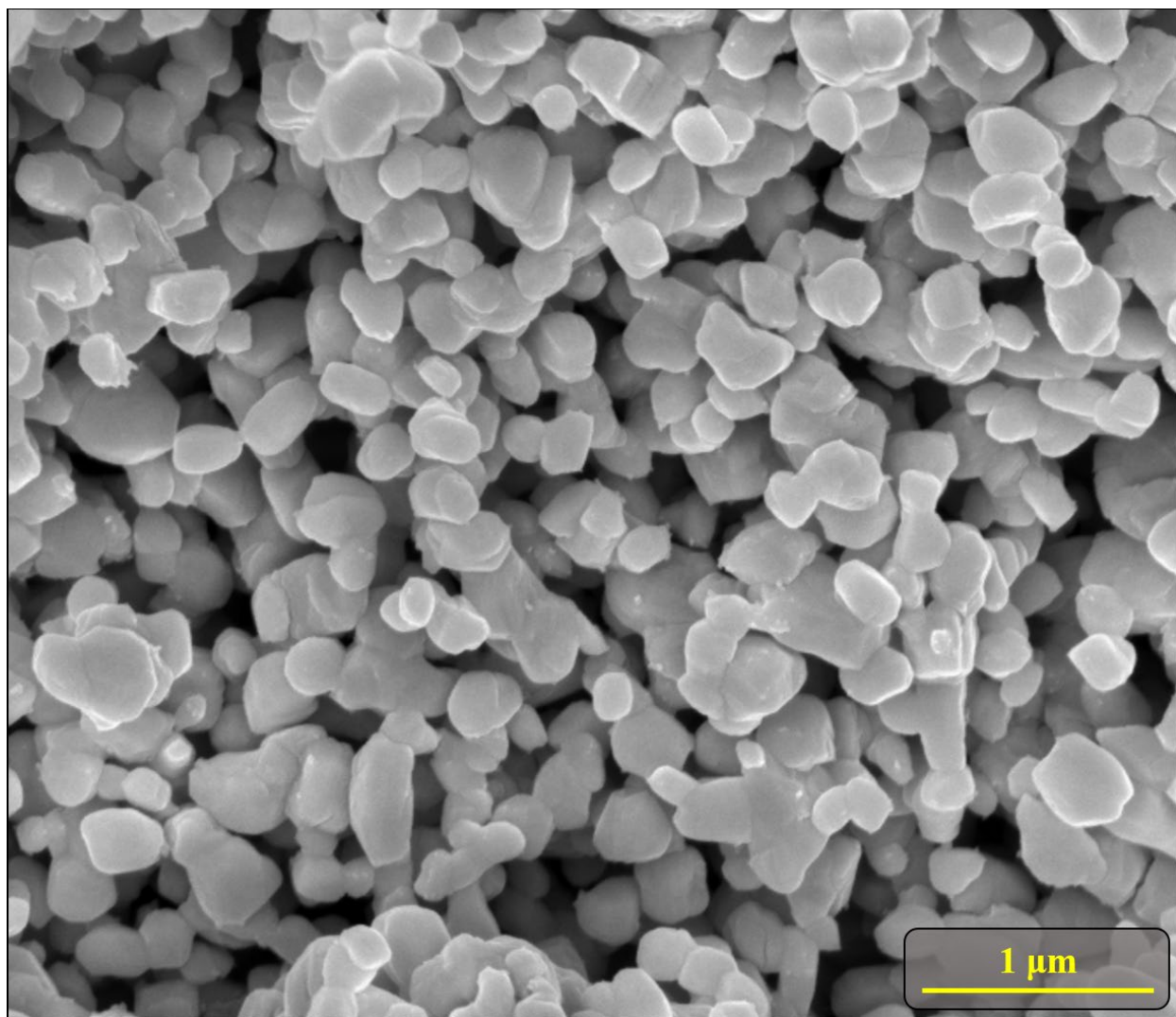


Figure S-19. SEM image representative of morphology of UO_2 synthesized from U_3O_8 as has been described in Figure S-14.

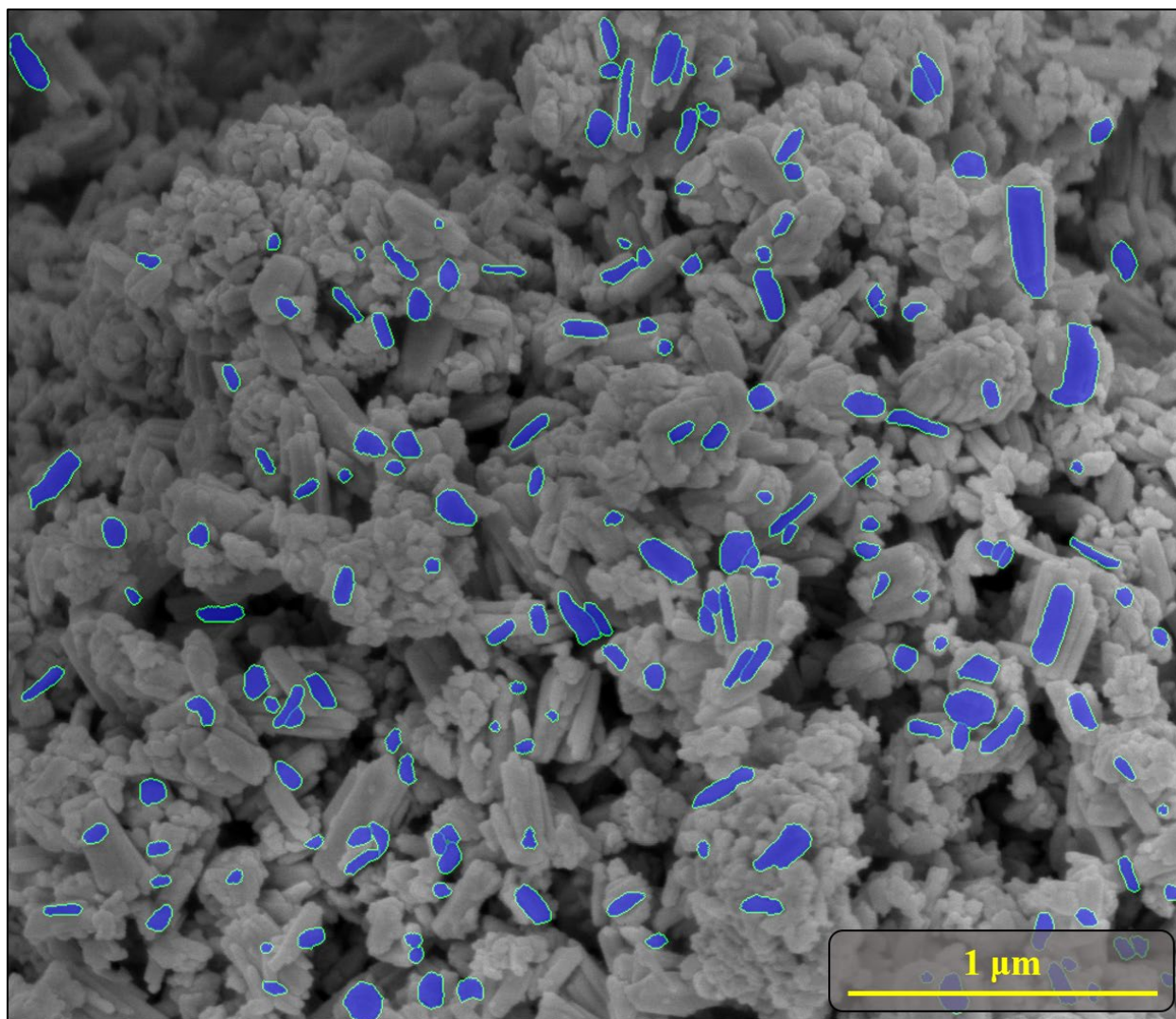


Figure S-20. An example of a segmented image of Am-UO₃. Using the MAMA software nano-particles are segmented to identify, isolate, and measured. Images were segmented using the procedure established by Olsen et al. to identify and isolate nano-particles for segmentation [1].

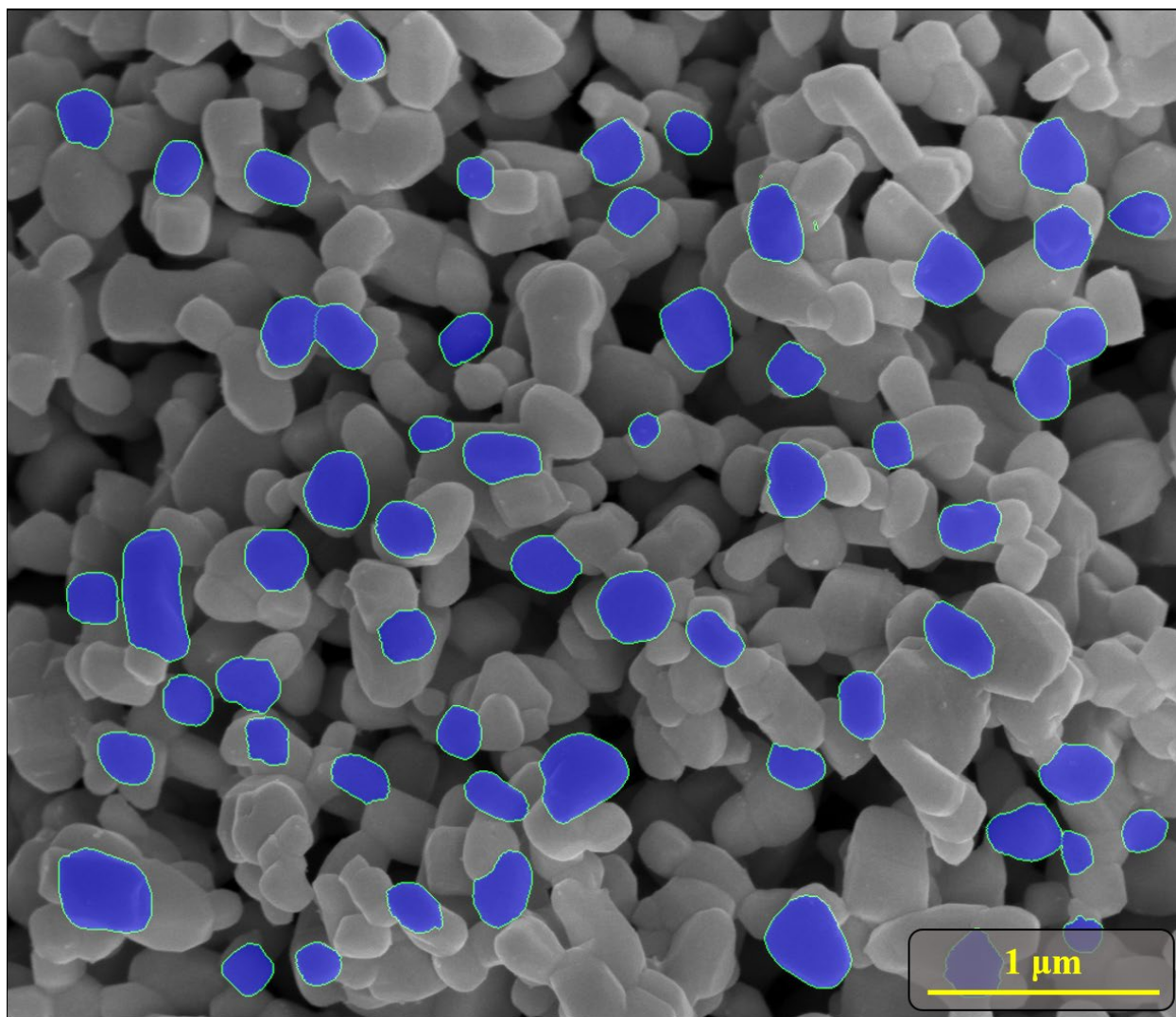


Figure S-21. An example of a segmented image of U_3O_8 . Using the MAMA software nano-particles are segmented to identify, isolate, and measured. Images were segmented using the procedure established by Olsen et al. to identify and isolate nano-particles for segmentation [1].

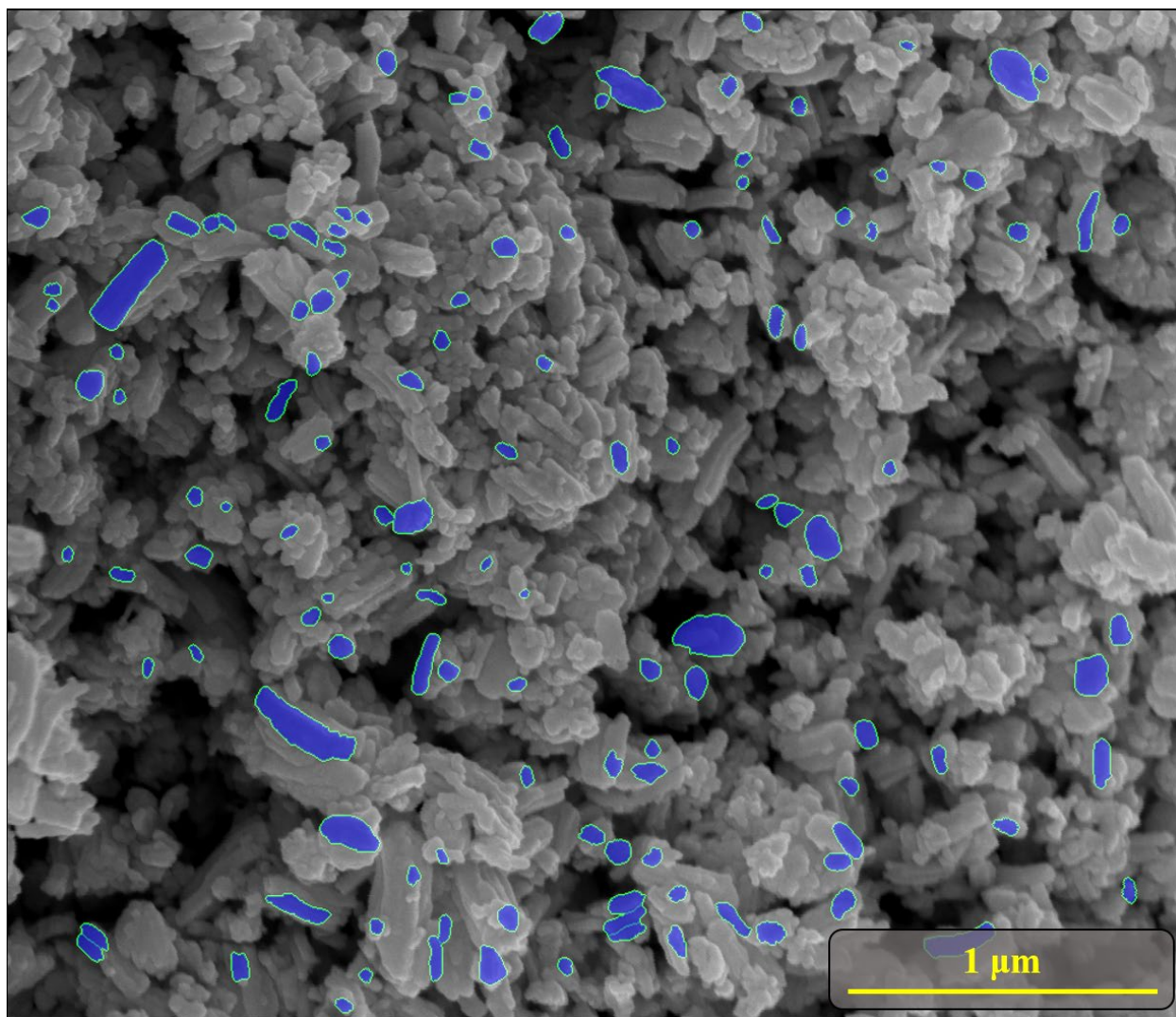


Figure S-22. An example of a segmented image of UO₂ synthesized from Am-UO₃. Using the MAMA software nano-particles are segmented to identify, isolate, and measured. Images were segmented using the procedure established by Olsen et al. to identify and isolate nano-particles for segmentation [1].

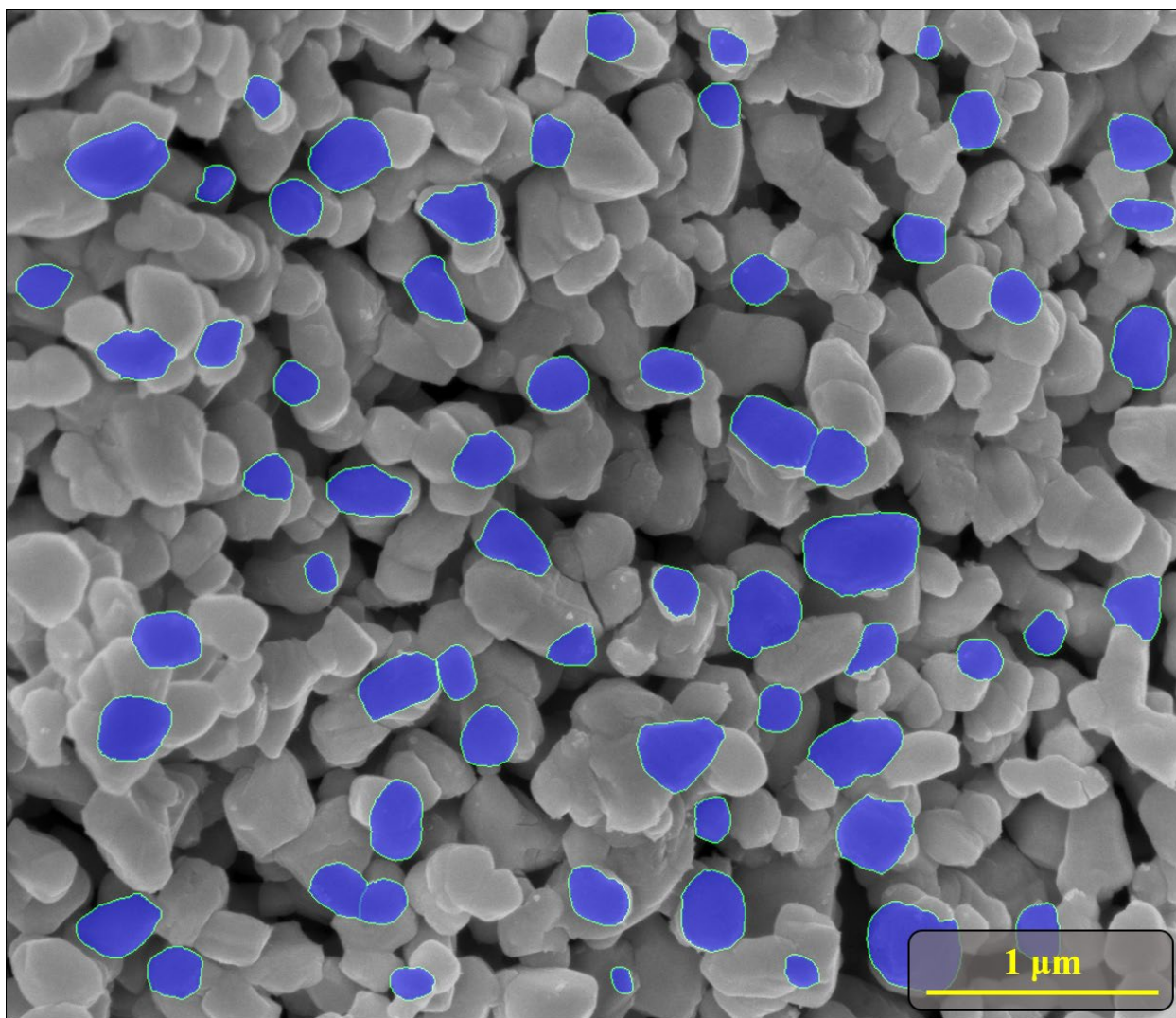


Figure S-23. An example of a segmented image of UO_2 synthesized from U_3O_8 . Using the MAMA software nano-particles are segmented to identify, isolate, and measured. Images were segmented using the procedure established by Olsen et al. to identify and isolate nano-particles for segmentation [1].

References

1. Olsen, A.M., Richards, B., Schwerdt, I., Heffernan, S., Lusk, R., Smith, B., Jurrus, E., Ruggiero, C., McDonald IV, L.W.: Quantifying morphological features of $\alpha\text{-U}_3\text{O}_8$ with image analysis for nuclear forensics. *Anal. Chem.* **89**, 3177 (2017).